Kobayashi, S., Stoten, D. P., Yamashita, Y., & Usuda, T. (2019). Dynamically substructured testing of railway pantograph/catenary systems. *Proceedings of the Institution of Mechanical Engineers, Part F: Journal of Rail and Rapid Transit*, *233*(5), 516-525. https://doi.org/10.1177/0954409718799900

Article type: Original article

Corresponding author:

Shigeyuki Kobayashi, Railway Technical Research Institute, 2-8-38 Hikari-cho, Kokubunji-shi, Tokyo, 185-8540, Japan

E-mail: kobayashi.shigeyuki.30@rtri.or.jp

Dynamically substructured testing of railway pantograph/catenary systems

Shigeyuki KOBAYASHI[1,2], David P. STOTEN[1], Yoshitaka YAMASHITA[2], Takayuki USUDA[2].

1 Advanced Control and Test Laboratory (ACTLab), Department of Mechanical Engineering, University of Bristol, Bristol BS8 1TR, United Kingdom.

2 Current Collection Laboratory, Railway Dynamics Division, Railway Technical Research Institute, Tokyo 1858540, Japan.

Abstract

This paper presents a methodology for testing railway pantograph/catenary systems based upon the dynamically substructured system (DSS) approach for combined physical and numerical components, originally developed by Stoten and Hyde. The main advantage of DSS is that it can provide more stable substructured testing than alternative schemes, such as the commonly used hybrid simulation method, often referred to as hardware-in-the-loop simulation. The developed method is validated through experiments using a simple

pantograph rig, together with a numerical simulation of the catenary. In order to realise a real-time simulation of the large catenary model, for the first time in DSS testing this study uses (I) a modal analysis technique to reduce the dimension of the contact wire model and (II) a moving window approach to represent long-distance travel of the pantograph. Finally, the experimental DSS test results are compared with simulations of the benchmark pantograph/catenary emulated system.

Keywords

Pantograph, overhead catenary system, dynamically substructured system, automatic control

Introduction

A typical current collection system that consists of a catenary and a pantograph is shown in Figure 1. When a vehicle is stationary the contact force between the pantograph head and contact wire is constant. However, this force fluctuates when the vehicle is running, mainly due to the presence of the catenary wire support points and droppers. In general, higher operating speeds of vehicles cause larger contact force fluctuations and therefore it is necessary that the current collection performance is improved in such cases. To place the current work in context, a brief review of relevant test systems is provided below.

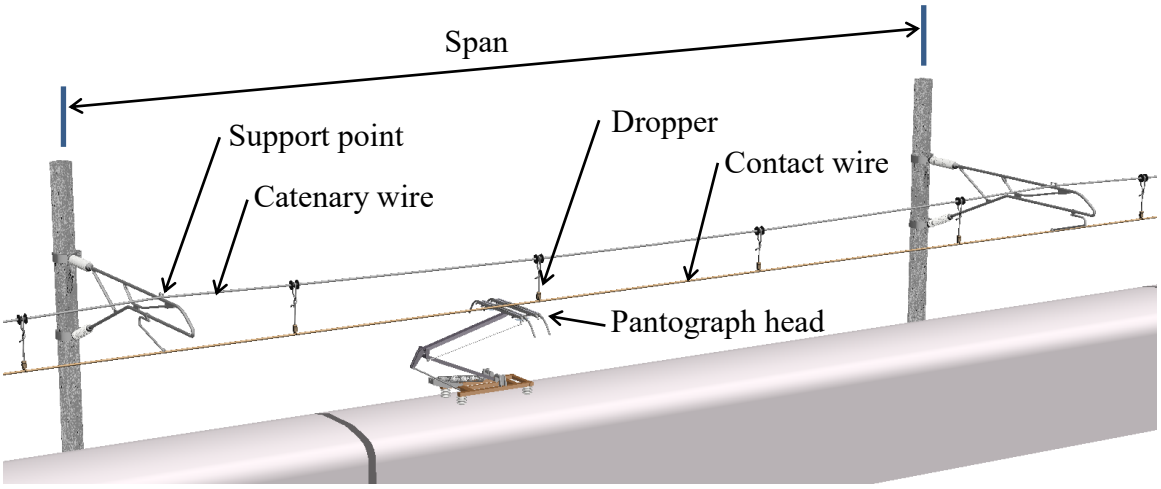

Figure 1. A typical overhead catenary and pantograph system.

One example of current collection performance enhancement for high-speed railways in Japan is the relatively simple expedient of dividing the contact strip on the pantograph head into separate small-mass sections. These can improve the dynamic compliance of the pantograph to prevent contact loss[1]. An actively controlled pantograph is also being developed[2], where the contact force is ideally made equal to the static uplift force generated by a raising mechanism on the pantograph. Feedback and/or feedforward techniques are being used to control the force to be equal to this static value.

Nevertheless, it is also vital that current collection performance is evaluated by a process of testing, with due consideration to the dynamic interaction between the pantograph

and catenary. After establishing the current collection function of pantographs, their performance can then be validated via on-track testing. However, this requires higher labour costs, track availability and, due to the high-voltage environment, problematic signal acquisition. Therefore, a laboratory-based testing scheme is the preferred option.

Dynamic characteristics of pantographs *per se* can be examined using the laboratory-based testing rig developed at the Tokyo-based Railway Technical Research Institute (RTRI)[2]. This essentially consists of a horizontal rotating disc together with an attached concentric contact track and the pantograph itself. The disc can be actuated in the vertical direction to simulate contact wire displacement and in the radial direction to simulate catenary stagger. Although the system provides for maximum vehicle speeds of 300 km/h, it cannot measure the essential dynamic interaction between the pantograph and the catenary. In this case, the vertical motion of the disc is determined by a predefined signal.

Therefore, alternative test equipment has been developed at the RTRI to measure this dynamic interaction[3], consisting of a tracked running device (representing the vehicle) that supports a pantograph and a linear catenary of length 400 m. This equipment can evaluate current collection performance, but the maximum velocity of the running device is limited to 200 km/h, which is not always sufficient for high-speed railway investigations. Moreover, the ‘coasting section’ of the track is approximately 70 m long, which is not always of

sufficient length for higher speed investigations. Although not laboratory-based in a conventional sense, this field system is located within the grounds of the RTRI.

Purely numerical techniques for pantograph/catenary systems are also being developed and they are used to understand the behaviour of the pantograph/catenary systems. Song, Liu, *et al*[4] have developed nonlinear finite element model of the catenary based upon cable and truss elements. Furthermore, wind-induced vibration has been analysed using a computational fluid dynamics software[5, 6]. An optimisation of existing catenary systems has been carried out by constructing a three dimensional finite element model[7]. In this case it was found that a 23 % increase in speed is available when a small pre-sag catenary is adopted. Variation in predicting the pantograph/catenary interaction has been surveyed by comparing simulation results and field measurements[8]. This study has demonstrated the effect of low-pass filtering for the contact force that is stipulated in the EN 50317:2012 standard. In order to understand the behaviour of pantograph/catenary systems, wave propagation analysis of the catenary is also used by Van, Massat, *et al*[9]. This study has pointed out that waves in the catenary wire are fully reflected, while reflections on the steady arm are negligible. Therefore, it is shown that dynamic characteristics of the droppers adjacent to the support point are important. Song, Liu, *et al*[10] have analysed the effect of the contact and catenary wire tensions on the wave reflection and transmission at the dropper points. A 3-dimensional finite element

model of the catenary with a lumped mass model of the pantograph, which includes their dynamic interaction, has been applied to the evaluation of the current collection performance at the RTRI[11]. However, it is recognised that system component modelling errors can have a significant effect on the accuracy of the numerical simulation.

As a direct consequence of the above, interest in substructured testing of railway pantograph/catenary systems has emerged in order to (i) improve current collection performance, (ii) improve operating speeds of vehicles and (iii) allow realistic testing within a laboratory environment. In particular, the use of the dynamically substructured system (DSS) testing method of Stoten and Hyde[12] is being investigated - research that forms the kernel of this paper.

In the next section, *'Substructure testing'*, the basic concepts of mixed physical/numerical component testing are introduced, along with specific details relevant to railway pantograph/catenary systems. Then, in *'The catenary model'*, the numerically modelled component of the substructured test is introduced, along with two methods of reducing its dynamic complexity in order to execute simulations in real-time. In the following two sections, *'The dynamically substructured system'* and *'Linear substructuring control design'*, the formulation of the DSS method is presented, together with the control algorithm that ensures DSS synchronisation of the physical pantograph head and the numerical contact

wire, at their point of virtual contact. This leads on to *'Experimental studies'*, detailing the main results of implementation tests on a DSS pantograph/catenary system, together with benchmark comparisons against simulated results. Finally, *'Conclusions'* presents the main outcomes to emerge from this work.

Substructure testing

As outlined in the *'Introduction'*, existing RTRI test systems have certain advantages and disadvantages. The various disadvantages have provided an impetus for the use of substructured system testing, thus enabling accurate, real-time investigations within a laboratory environment. At RTRI, a pantograph testing rig has been constructed to test the DSS method. It consists of a shinkansen pantograph, a servo-controlled actuator system for the pantograph and a real-time numerical simulator/substructure controller; see Figure 2. In this configuration, the catenary displacement is calculated by the real-time numerical simulator, which in turn is fed by the contact force measurement. Using the same discrete-time hardware, a substructure control algorithm generates a displacement demand signal to the inner-loop servo controller that, by design, ensures any difference between the numerical (catenary) and physical (pantograph) displacements is driven towards zero. In principle, the

outer-loop substructure control algorithm can be of any suitable type and this issue is discussed in a subsequent section. Similarly, the inner-loop displacement servo controller can also be of any type, but it is typically based upon a conventional proportional-integral-derivative (PID) algorithm.

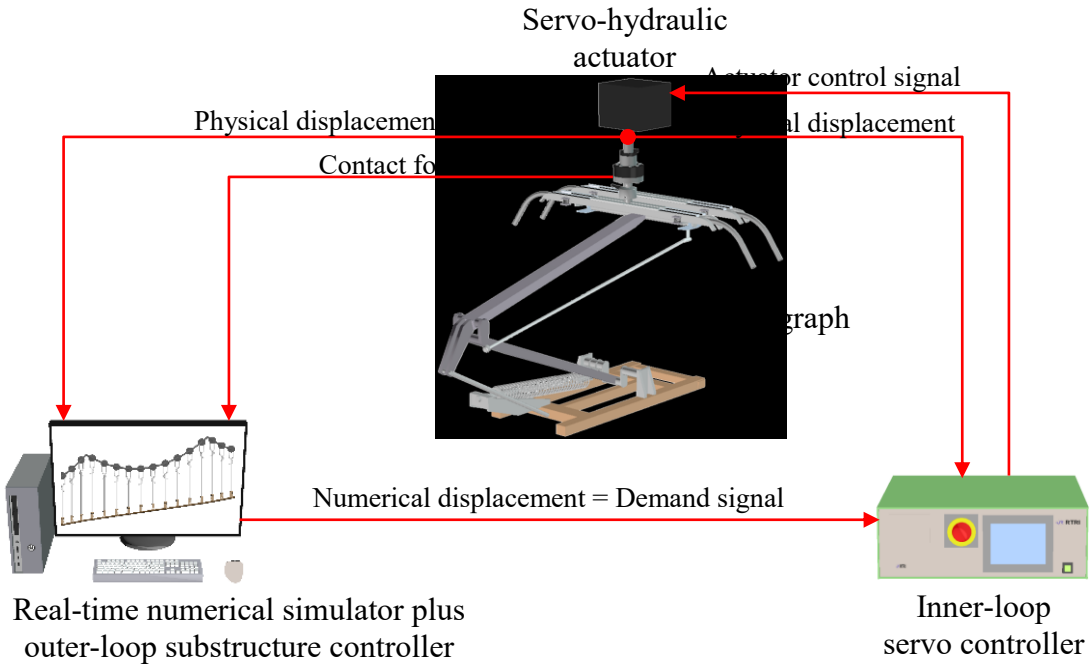

Figure 2. A schematic image of the substructured pantograph/catenary testing system.

Substructured testing can be classified into hardware-in-the-loop simulation (HiLS), hybrid simulation (HS) and dynamically substructured system (DSS)[13] methods, where the terminology is often used in an equivocal manner. For example, the expressions HiLS and HS are often used synonymously. Substructured testing for the pantograph/catenary systems based on HS has already been extensively developed and used, e.g. Facchinetti, Gasparetto, *et al*[14] and Schirrer, Aschauer, *et al*[15].

Since DSS can provide significantly higher stability margins than HS[13], the RTRI and the University of Bristol have applied the DSS testing method to a simplified representation of a physical pantograph, called the quasi-pantograph (QP), that is linked with a numerical catenary system. Successful DSS designs are then transferred directly from the QP to the substructured pantograph testing rig at the RTRI.

The original QP rig used a mass-spring-damper (*m*-*k*-*c*) single degree-of-freedom (SDOF) mechanism to represent the pantograph and an entirely different *m*-*k*-*c* SDOF numerical model for the catenary[16, 17]. The configuration of the developed substructured system is shown in Figure 3, where the modelled catenary spring term has a time-variant stiffness that represents equivalent changes in the catenary due to movement of the pantograph along a virtual track. Although it enabled both stable testing and a representation

of long-distance travel of the pantograph, the SDOF catenary model could not simulate wave propagation of vertical displacement along the wires.

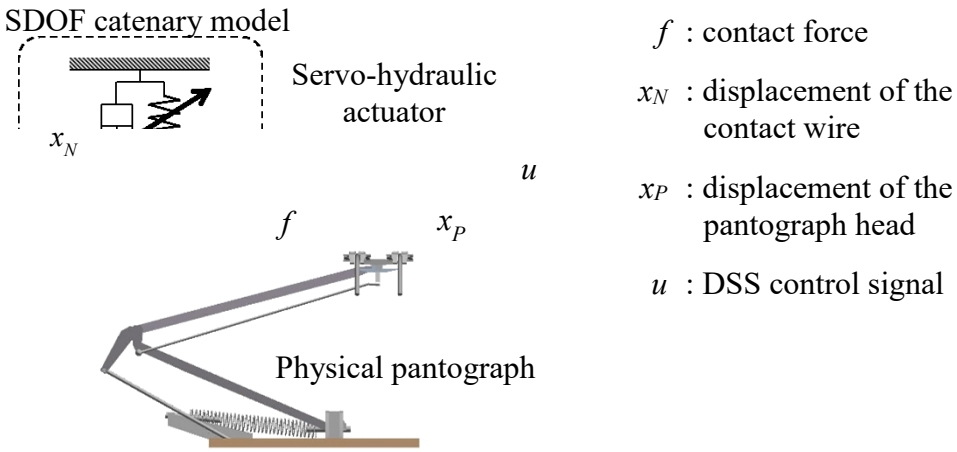

Figure 3. The original SDOF catenary-based QP-DSS testing system.

Thus, a multi degree-of-freedom (MDOF) catenary model was subsequently used within the DSS method[18], where the catenary was modelled as a lumped mass system; see Figure 4. By indexing the location of the point of application of the contact force (shown as the red arrow in the figure), the pantograph behaved as if it was running beneath the catenary. Furthermore, it was now possible to investigate wave propagation within the catenary model. However, due to the dynamic complexity, it was not possible to compute the real-time response of a catenary model with more than 5 spans. Hence, one of the main purposes of this paper is to present an MDOF catenary-based DSS method that can represent much

longer-distance travel of pantographs. In order to do this, the basis of the associated catenary model and associated model reduction methods are presented in the next section.

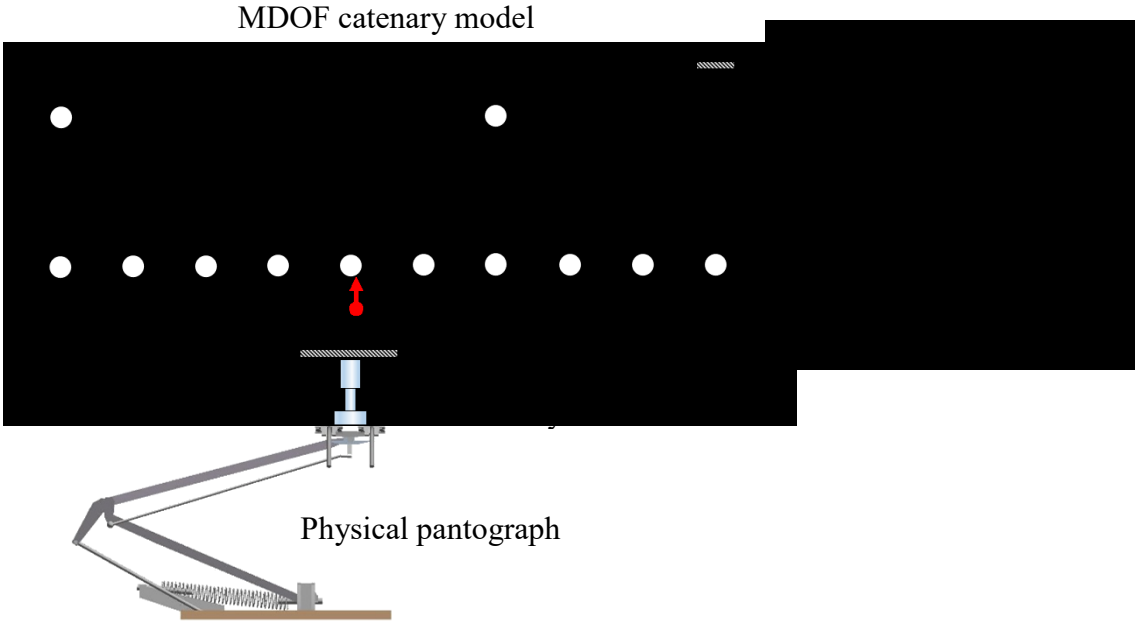

Figure 4. The MDOF catenary-based QP-DSS testing system.

The catenary model

Model overview

The catenary system is modelled as a lumped mass system as shown in Figure 5, where both the catenary wire and contact wire are divided into discrete masses connected via parallel springs and dashpots. Although catenary wire masses are defined only at locations where droppers exist, contact wire masses are defined over 6 equal intervals between adjacent droppers. The terminations of both contact and catenary wires and the support points of the catenary wire are rigidly fixed. In addition, the tensioned wires are represented by springs and the droppers by springs and dashpots.

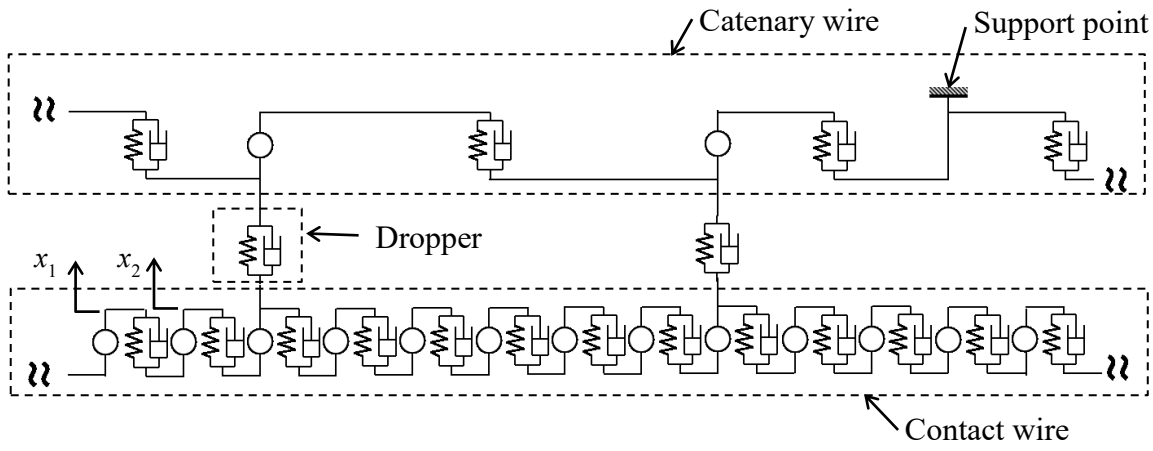

Figure 5. The MDOF catenary model, based upon a lumped mass system.

A specification of the catenary model that is used in this paper is summarised in Table 1.

Table 1. A specification of the catenary model.

Catenary wire	Tensile force	19600 N
	Mass per unit length	1.375 kg/m
Contact wire	Tensile force	19600 N
	Mass per unit length	0.935 kg/m
Span length		50 m
Dropper interval		5 m

Model reduction methods

It is essential that substructured testing realises long-distance travel of a pantograph. However, since this would require a very large and complex catenary model, where the response would be difficult to calculate in real-time using conventional laboratory hardware and software. Therefore, this study uses (I) a modal analysis technique and (II) a moving window approach to reduce the dimension of the catenary model, thereby allowing for real-time computation of its response.

(I) Modal analysis technique

Since the dimension of the catenary wire is relatively low, although it is modelled in physical coordinates, its response can be solved in real-time. However, the dimension of the contact wire is too large to simulate in real-time and therefore it is modelled in modal coordinates, thereby providing the first method of model reduction.

Thus, the equation of motion of the MDOF contact wire model is represented in physical coordinates as:

$$\mathbf{M}\ddot{\mathbf{x}} + \mathbf{C}\dot{\mathbf{x}} + \mathbf{K}\mathbf{x} = \mathbf{f} \tag{1}$$

where **M**, **C** and **K** are the ($n \times n$) mass, damping and stiffness matrices, respectively. Furthermore, **f** is the external force vector that is applied to the contact wire and $\mathbf{x} = [x_1, x_2, \ldots, x_n]^{\mathrm{T}}$, where x_i are displacement of masses of the contact wire model. In addition, the generalized eigenvalue problem is represented by

$$\left(\Omega^2 \mathbf{M} - \mathbf{K}\right)\mathbf{X} = \mathbf{0} \tag{2}$$

where **X** is a complex amplitude of $\mathbf{x}(t)$ at the angular frequency Ω.

In order to reduce the dimension of the contact wire model, the displacement vector in physical coordinates, $\mathbf{x}(t)$, is approximately represented by the first r ($r < n$) eigenmodes as follows:

$$\mathbf{x}(t) \approx \boldsymbol{\Phi}_{\mathbf{r}}\, \xi_{\mathbf{r}}(t) \tag{3}$$

where the r columns of the matrix $\boldsymbol{\Phi}_{\mathbf{r}}$ consist of the ordered eigenvectors and $\xi_{\mathbf{r}}(t)$ is the corresponding modal displacement vector. By substituting the coordinate transformation equation (3) into equation (1) and pre-multiplying by $\boldsymbol{\Phi}_{\mathbf{r}}{}^{\mathrm{T}}$, the equation of motion of the contact wire is obtained in modal coordinates as:

$$\boldsymbol{\Phi}_{\mathbf{r}}{}^{\mathrm{T}}\, \mathbf{M} \boldsymbol{\Phi}_{\mathbf{r}}\, \ddot{\xi} + \boldsymbol{\Phi}_{\mathbf{r}}{}^{\mathrm{T}}\, \mathbf{C} \boldsymbol{\Phi}_{\mathbf{r}}\, \dot{\xi} + \boldsymbol{\Phi}_{\mathbf{r}}{}^{\mathrm{T}}\, \mathbf{K} \boldsymbol{\Phi}_{\mathbf{r}}\, \mathbf{x} = \boldsymbol{\Phi}_{\mathbf{r}}{}^{\mathrm{T}}\, \mathbf{f}. \tag{4}$$

The pre-multiplying terms on the left-hand side of equation (4) can be written as:

$$\mathbf{M}_{\mathbf{r}} = \boldsymbol{\Phi}_{\mathbf{r}}{}^{\mathrm{T}}\, \mathbf{M} \boldsymbol{\Phi}_{\mathbf{r}} \tag{5}$$

$$\mathbf{C}_{\mathbf{r}} = \boldsymbol{\Phi}_{\mathbf{r}}{}^{\mathrm{T}}\, \mathbf{C} \boldsymbol{\Phi}_{\mathbf{r}} \tag{6}$$

$$\mathbf{K}_{\mathbf{r}} = \boldsymbol{\Phi}_{\mathbf{r}}{}^{\mathrm{T}}\, \mathbf{K} \boldsymbol{\Phi}_{\mathbf{r}} \tag{7}$$

where $\mathbf{M_r}$, $\mathbf{C_r}$ and $\mathbf{K_r}$ are diagonal ($r \times r$) modal mass, damping and stiffness matrices, respectively. Substituting equations (5), (6) and (7) into equation (4), the equation of motion can finally be rewritten as follows:

$$\mathbf{M}_r \ddot{\mathbf{x}} + \mathbf{C}_r \dot{\mathbf{x}} + \mathbf{K}_r \mathbf{x} = \mathbf{\Phi}_r^{\mathrm{T}} \mathbf{f} \tag{8}$$

Since a focus of this study is on the fundamental principles of substructure testing for pantograph/catenary systems, this paper assumes that the catenary model does not have significant nonlinearity, especially due to slackening of the droppers. This effect will be introduced in our future work.

(II) Moving window approach

The moving window approach was originally introduced by Facchinetti, Gasparetto, *et al*[14]. Here, the complex catenary model is divided into a set of smaller catenary models as shown in Figure 6, where each smaller model is successively used in the real-time simulation. As described previously, the number of spans within each smaller model should be no more than 5; in this study just 3 spans are used within each window.

The ends of the wires of the smaller model are fixed. Simulation results presented in the section 'Comparison of experimental and emulated system results' show good correspondence between experimental and simulated results, in spite of the relatively simple boundary conditions.

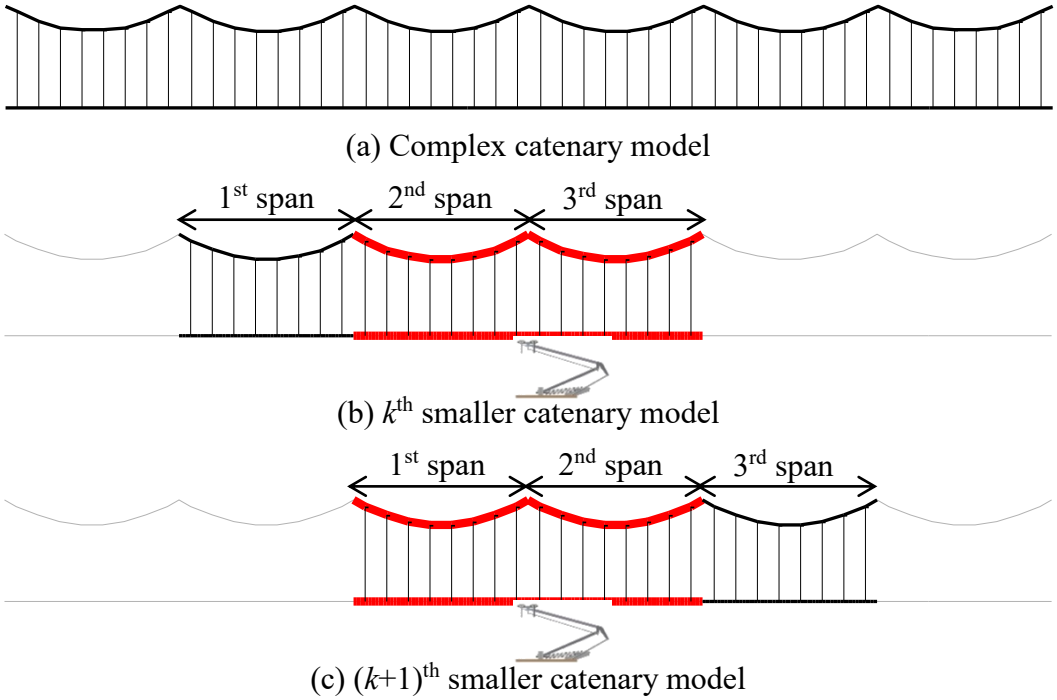

(a) Complex catenary model

(b) k^{th} smaller catenary model

(c) $(k+1)^{th}$ smaller catenary model

Figure 6. A schematic diagram of the moving window approach.

The scheme proceeds as follows. When the pantograph arrives at the left side of the 3^{rd} span of the k^{th} model, both displacement and velocity of the 2^{nd} and 3^{rd} span of the k^{th} model are copied to the 1^{st} and 2^{nd} span of the $(k+1)^{th}$ model. Then, it is assumed that the displacement of the 3^{rd} span of the $(k+1)^{th}$ catenary model is approximated by its static displacement. Simultaneously, the location of the pantograph is moved from the left side of the 3^{rd} span of the k^{th} model to the left side of the 2^{nd} span of the $(k+1)^{th}$ model.

Although the above copying process of state variables is suitable for use with physical coordinates, i.e. for the catenary wire model, it also has to be applied to the contact wire model constructed in modal coordinates. Since the copying process requires coordinate transformation from modal to physical coordinates (and *vice versa*), even though the modal analysis technique is adopted, the time-history response of the contact wire model cannot be calculated in real-time due to the dynamic complexity. However, by applying linear algebraic operations to the copying process of the contact wire model, as given by the developments in Equations (9)-(18) below, the moving window approach can be used for the real-time simulation.

As shown in equation (3), the physical displacement of the contact wire of the k^{th} smaller catenary model $\mathbf{x}_{(k)} = [\mathbf{x}_{\mathbf{1}(k)}{}^{\mathrm{T}}, \mathbf{x}_{\mathbf{2}(k)}{}^{\mathrm{T}}, \mathbf{x}_{\mathbf{3}(k)}{}^{\mathrm{T}}]^{\mathrm{T}}$ can be represented using eigenvectors $\mathbf{\Phi}_{(k)}$ and the modal displacement $\boldsymbol{\xi}_{(k)}$:

$$\mathbf{x}_{(k)} = \mathbf{\Phi}_{(k)} \boldsymbol{\xi}_{(k)} \tag{9}$$

Displacement of the 2nd and 3rd span of the k^{th} smaller catenary model, $\mathbf{x}_{\mathbf{2}(k)}$ and $\mathbf{x}_{\mathbf{3}(k)}$, are copied to those of the 1st and 2nd span of the $(k+1)^{\text{th}}$ model, $\mathbf{x}_{\mathbf{1}(k+1)}$ and $\mathbf{x}_{\mathbf{2}(k+1)}$, as follows:

$$\underbrace{\begin{Bmatrix} \mathbf{x}_{\mathbf{1}(k+1)} \\ \mathbf{x}_{\mathbf{2}(k+1)} \\ \mathbf{0} \end{Bmatrix}}_{\bar{\mathbf{x}}_{(k+1)}} = \begin{Bmatrix} \mathbf{x}_{\mathbf{2}(k)} \\ \mathbf{x}_{\mathbf{3}(k)} \\ \mathbf{0} \end{Bmatrix} = \underbrace{\begin{bmatrix} \mathbf{0} & \mathbf{I} & \mathbf{0} \\ \mathbf{0} & \mathbf{0} & \mathbf{I} \\ \mathbf{0} & \mathbf{0} & \mathbf{0} \end{bmatrix}}_{\mathbf{T}} \underbrace{\begin{Bmatrix} \mathbf{x}_{\mathbf{1}(k)} \\ \mathbf{x}_{\mathbf{2}(k)} \\ \mathbf{x}_{\mathbf{3}(k)} \end{Bmatrix}}_{\mathbf{x}_{(k)}} \tag{10}$$

Then, equation (10) is rewritten as

$$\bar{\mathbf{x}}_{(k+1)} = \mathbf{T}\,\mathbf{x}_{(k)} \tag{11}$$

Equation (12) is then obtained by substitution of equation (11) into equation (9):

$$\overline{\mathbf{x}}_{(k+1)} = \mathbf{T}\,\boldsymbol{\Phi}_{(k)}\,\boldsymbol{\xi}_{(k)} \tag{12}$$

Furthermore, displacement of the 3rd span of the $(k+1)^{th}$ model is set as the static displacement $\mathbf{x_3(0)}_{(k+1)}$, based upon the following equation:

$$\begin{Bmatrix} \mathbf{x_1}_{(k+1)} \\ \mathbf{x_2}_{(k+1)} \\ \mathbf{x_3}_{(k+1)} \end{Bmatrix} = \begin{Bmatrix} \mathbf{0} \\ \mathbf{0} \\ \mathbf{x_3(0)}_{(k+1)} \end{Bmatrix} + \begin{Bmatrix} \mathbf{x_1}_{(k+1)} \\ \mathbf{x_2}_{(k+1)} \\ \mathbf{0} \end{Bmatrix} = \mathbf{x(0)}_{(k+1)} + \overline{\mathbf{x}}_{(k+1)} \tag{13}$$

Using the coordinate transformation $\mathbf{x(0)}_{(k+1)} = \boldsymbol{\Phi}_{(k+1)}\,\boldsymbol{\xi(0)}_{(k+1)}$ and substituting equation (12) into equation (13), the displacement of the $(k+1)^{th}$ model, $\mathbf{x}_{(k+1)}$, is derived from the physical coordinates as:

$$\mathbf{x}_{(k+1)} = \boldsymbol{\Phi}_{(k+1)}\,\boldsymbol{\xi(0)}_{(k+1)} + \mathbf{T}\,\boldsymbol{\Phi}_{(k)}\,\boldsymbol{\xi}_{(k)} \tag{14}$$

Here, $\boldsymbol{\xi(0)}_{(k+1)}$ is the static displacement of the $(k+1)^{th}$ model in modal coordinates. Finally, the physical displacement $\mathbf{x}_{(k+1)}$ is transformed into modal coordinates by equation (15):

$$\boldsymbol{\xi}_{(k+1)} = \boldsymbol{\Phi}^{\mathrm{T}}{}_{(k+1)}\,\mathbf{M}_{(k+1)}\,\mathbf{x}_{(k+1)} \tag{15}$$

where $\mathbf{M}_{(k+1)}$ is the modal mass matrix of the $(k+1)^{\text{th}}$ catenary model and $\boldsymbol{\Phi}_{(k+1)}$ is a matrix that consists of the normalised eigenvectors, as follows:

$$\boldsymbol{\Phi}^{\mathrm{T}}{}_{(k+1)}\,\mathbf{M}_{(k+1)}\,\boldsymbol{\Phi}_{(k+1)} = \mathbf{I} \tag{16}$$

Substituting equation (14) into equation (15) and using equation (16), the modal displacement of the k^{th} catenary model can be copied to the $(k+1)^{\text{th}}$ catenary model as follows:

$$\begin{aligned}\boldsymbol{\xi}_{(k+1)} &= \boldsymbol{\Phi}^{\mathrm{T}}{}_{(k+1)}\,\mathbf{M}_{(k+1)}\left(\boldsymbol{\Phi}_{(k+1)}\,\boldsymbol{\xi}_{\mathbf{0}(k+1)} + \mathbf{T}\,\boldsymbol{\Phi}_{(k)}\,\boldsymbol{\xi}_{(k)}\right)\\ &= \boldsymbol{\Phi}^{\mathrm{T}}{}_{(k+1)}\,\mathbf{M}_{(k+1)}\,\boldsymbol{\Phi}_{(k+1)}\,\boldsymbol{\xi}_{\mathbf{0}(k+1)} + \boldsymbol{\Phi}^{\mathrm{T}}{}_{(k+1)}\,\mathbf{M}_{(k+1)}\,\mathbf{T}\,\boldsymbol{\Phi}_{(k)}\,\boldsymbol{\xi}_{(k)}\\ &= \boldsymbol{\xi}_{\mathbf{0}(k+1)} + \mathbf{A}\,\boldsymbol{\xi}_{(k)}\end{aligned} \tag{17}$$

where

$$\mathbf{A} = \boldsymbol{\Phi}^{\mathrm{T}}{}_{(k+1)}\,\mathbf{M}_{(k+1)}\,\mathbf{T}\,\boldsymbol{\Phi}_{(k)} \tag{18}$$

In equation (17), both $\boldsymbol{\xi(0)}_{(k+1)}$ and **A** can be calculated *a priori*. Therefore, the copying process based upon equation (17) is faster than the coordinate transformation from modal to physical coordinates and *vice versa*.

The dynamically substructured system

In the DSS method, the pantograph/catenary system is divided into a physical substructure and a numerical substructure. The pantograph is defined as the physical substructure and the catenary is defined as the numerical substructure; see Figure 7. Here, the physical substructure is labelled as Σ_P, which is driven by a hydraulic actuator that is labelled as Σ_A, and the numerical substructure is labelled as Σ_N. The actuator is driven by the substructuring control signal, u, which in turn generates the actuator ram displacement, x_P. This ram displacement is identical to that of the pantograph head, since the two are rigidly connected for all implementation tests described in this work.

In addition, the contact force between the two components, f, is measured using a load cell that, together with x_P, is input to the numerical contact wire model. The mass index, i, of the contact wire model – the point at which the contact force is applied – changes with time due to the travelling pantograph. For example, Figure 7 shows the pantograph located

beneath the i^{th} mass of the contact wire model, with displacement x_i and the measured contact force (shown in red) also being applied at this point.

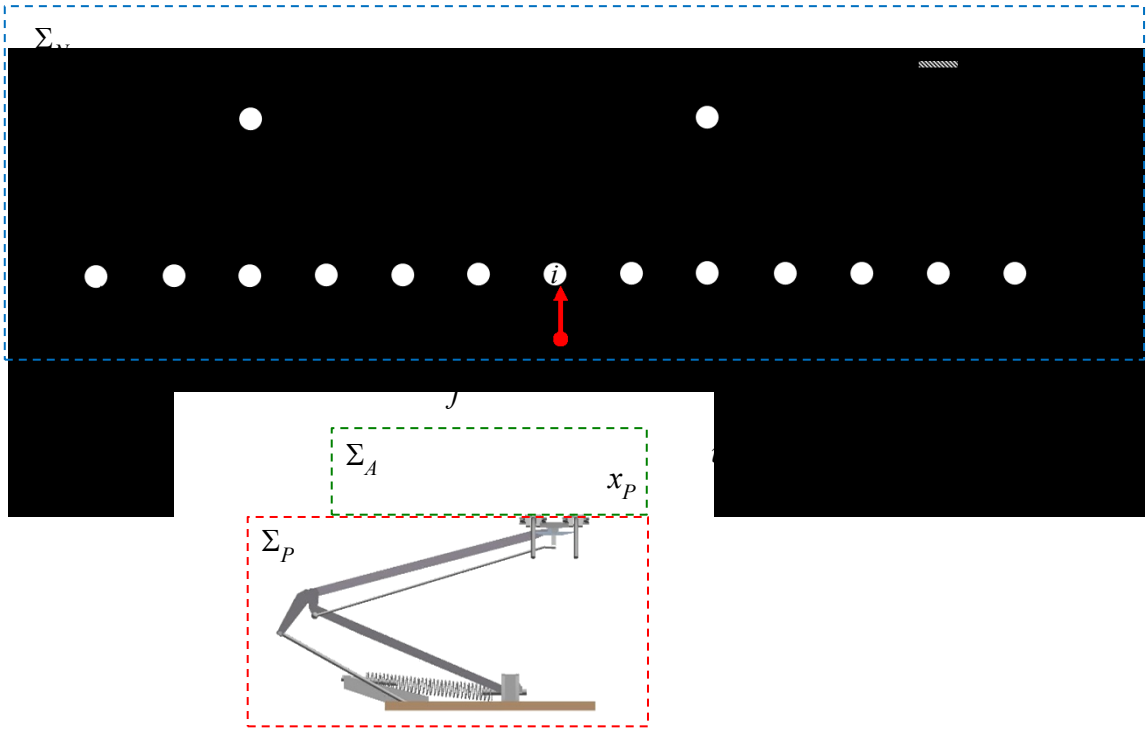

Figure 7. A pantograph/catenary substructured system, using DSS terminology.

DSS can be synthesised via a transfer function or a state-space approach. Since the number of DOF of the catenary model tends to be high (typically ~360), its transfer function would tend to be numerically ill-conditioned. Therefore, DSS design is executed via the more well-conditioned state-space approach of Tu, Stoten, *et al*[19] in this paper. Hence, using physical coordinates, the equation of motion of the contact wire is written in state-space form as:

$$\begin{bmatrix} \dot{\mathbf{x}}_{N1} \\ \dot{\mathbf{x}}_{N2} \end{bmatrix} = \begin{bmatrix} -\mathbf{M}^{-1}\mathbf{C} & \mathbf{I} \\ -\mathbf{M}^{-1}\mathbf{K} & \mathbf{0} \end{bmatrix} \begin{bmatrix} \mathbf{x}_{N1} \\ \mathbf{x}_{N2} \end{bmatrix} + \begin{bmatrix} \mathbf{0} \\ \mathbf{M}^{-1} \end{bmatrix} \mathbf{f} = \begin{bmatrix} \mathbf{A}_{N11} & \mathbf{I} \\ \mathbf{A}_{N21} & \mathbf{0} \end{bmatrix} \begin{bmatrix} \mathbf{x}_{N1} \\ \mathbf{x}_{N2} \end{bmatrix} + \begin{bmatrix} \mathbf{0} \\ \mathbf{B}_{N2} \end{bmatrix} \mathbf{f} \tag{19}$$

where

$$\mathbf{x}_{N1} = \mathbf{x} \tag{20}$$

$$\mathbf{x}_{N2} = \mathbf{M}^{-1} \int_0^t \left(-\mathbf{K}\,\mathbf{x} + \mathbf{f} \right) dt \tag{21}$$

Over the bandwidth of interest, experimentation has shown that the actuator is adequately modelled as a first-order system:

$$\dot{x}_P = -a\,x_P + b\,u \tag{22}$$

where $a = 1/T$, $b = \lambda/T$, T is the time constant of the actuator and λ is its low frequency gain.

The dynamics of the DSS substructuring error, $x_{e(i)}$, i.e. the difference between the displacement of the contact wire model at the i^{th} mass, $x_{N1(i)}$, and the displacement of the actuator, x_P, can therefore be determined as:

$$\begin{aligned}\dot{x}_{e(i)} &= \dot{x}_{N1(i)} - \dot{x}_P \\ &= A_{N11(i,i)}x_{e(i)} + A_{N11(i,i-1)}x_{N1(i-1)} + A_{N11(i,i+1)}x_{N1(i+1)} + x_{N2(i)} + \Lambda \\ &\qquad \Lambda + \left(A_{N11(i,i)} + a\right)x_P - b\,u\end{aligned} \tag{23}$$

Equation (23) is valid for $2 \le i \le n$-1; where n is the number of masses within the contact wire model. Since both terminations of the catenary model are rigidly constrained, the pantograph dynamic model is not defined at location indices $i = 1$ and n.

In the next subsection, linear substructuring control (LSC)[19] is used to formulate a design that ensures the global asymptotic stability of the substructuring error, $x_{e(i)}$.

Linear substructuring control design

LSC is designed for each condition when the pantograph is located under the i^{th} mass of the contact wire. In order to ensure that the substructuring error is globally asymptotically stable, the control input, u, is defined as:

$$u = K_{e(i)}x_{e(i)} + K_{N1(i-1)}x_{N1(i-1)} + K_{N1(i+1)}x_{N1(i+1)} + K_{N2(i)}x_{N2(i)} + K_P x_P \tag{24}$$

where $K_{e(i)}$, $K_{N1(i\text{-}1)}$, $K_{N1(i+1)}$, $K_{N2(i)}$ and K_P are the LSC gains. Substituting equation (24) into equation (23), the error dynamics are obtained as

$$\begin{aligned}\dot{x}_{e(i)} = {} & \left(A_{N11(i,i)} - b\,K_{e(i)}\right)x_{e(i)} + \Lambda \\ & \Lambda + \left(A_{N11(i,i-1)} - b\,K_{N1(i-1)}\right)x_{N1(i-1)} + \left(A_{N11(i,i+1)} - b\,K_{N1(i+1)}\right)x_{N1(i+1)} + \Lambda \\ & \Lambda + \left(1 - b\,K_{N2(i)}\right)x_{N2(i)} + \left(A_{N11(i,i)} + a - b\,K_P\right)x_P\end{aligned} \tag{25}$$

where $K_{N1(i\text{-}1)}$, $K_{N1(i+1)}$, $K_{N2(i)}$ and K_P are determined so that second to fifth terms on the right-hand side of equation (25) are zero:

$$K_{N1(i-1)} = \frac{A_{N11(i,i-1)}}{b} \tag{26}$$

$$K_{N1(i+1)} = \frac{A_{N11(i,i+1)}}{b} \tag{27}$$

$$K_{N2(i)} = \frac{1}{b} \tag{28}$$

$$K_P = \frac{A_{N11(i,i)} + a}{b} \tag{29}$$

Substituting equations (26) to (29) into equation (25), the error dynamics are then given by the scalar homogeneous differential equation:

$$\dot{x}_{e(i)} = \left(A_{N11(i,i)} - b\,K_{e(i)}\right)x_{e(i)} \tag{30}$$

Numerous robust control designs can be used to determine a suitable $K_{e(i)}$ in equation (30), e.g. two commonly-used techniques are adaptive control[12] and H_∞ control[19]. Since the focus of this study is on the principles of DSS for pantograph/catenary systems, rather than on control design *per se*, a simple proportional control will suffice. Thus, given a required settling time of the first-order dynamics, t_s, $K_{e(i)}$ is determined from equation (30) as:

$$K_{e(i)} = \frac{A_{N11(i,i)} + 4/t_s}{b} \tag{31}$$

In this paper, it is assumed that all masses and dashpots of the contact wire model have identical coefficients. Therefore, $A_{N11(i,i)}$ does not depend on the index i and, as a consequence, the gains $K_{e(i)}$, $K_{N1(i\text{-}1)}$, $K_{N1(i+1)}$ and $K_{N2(i)}$ are constant and also independent of i.

Figure 8 shows a diagram of the complete DSS-LSC substructured system thereby obtained for the pantograph/catenary system. Since the QP is not equipped with a device to generate static uplift, an equivalent offset displacement is also provided by the actuator.

The main difference between HS and DSS is that DSS assumes dynamic characteristics of the actuator cannot be identified perfectly. Therefore, the substructuring error $x_{e(i)}$ has been introduced, which can be decreased via the proposed automatic control method. Furthermore, the eigenvalue of the DSS-LSC system can be designed by judicious selection of the controller gain, $K_{e(i)}$.

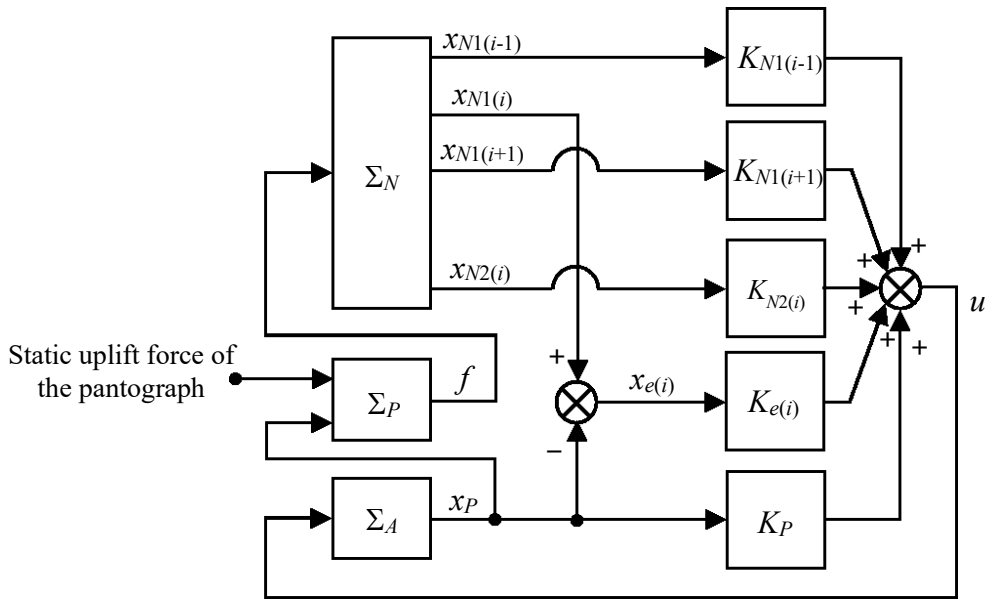

Figure 8. Block diagram of the pantograph/catenary DSS-LSC system.

Experimental studies

In this section, the DSS performance is evaluated via experimental substructured tests conducted on the QP rig at the University of Bristol. The benchmark emulated (i.e overall) system is also simulated numerically and the results compared with the experimental responses.

Figure 9 shows the simple mechanical system that constitutes the QP rig, consisting of a mass, a spring and damping that is inherent to the mechanism, whilst Figure 10 shows a block diagram of the complete DSS implementation. One side of the QP is rigidly supported, and the other is driven by the servo-controlled hydraulic actuator, with an inner-loop Instron 8800 controller running a displacement proportional (P) control law. The contact force between the pantograph/catenary systems, f, is measured by a load cell that is introduced between the QP and the actuator. The measured force is then input via an A/D converter to the real-time numerical model of the contact wire, simulated on a dSPACE DS1104 processor. In addition, the measured displacement of the QP, x_P, is fed back to both the Instron controller and the dSPACE processor, which also has the task of running the DSS-LSC algorithm. The resulting LSC control signal, u (i.e. the displacement demand to the Instron controller), is output from the dSPACE processor via a D/A converter. This completes the closed-loop system.

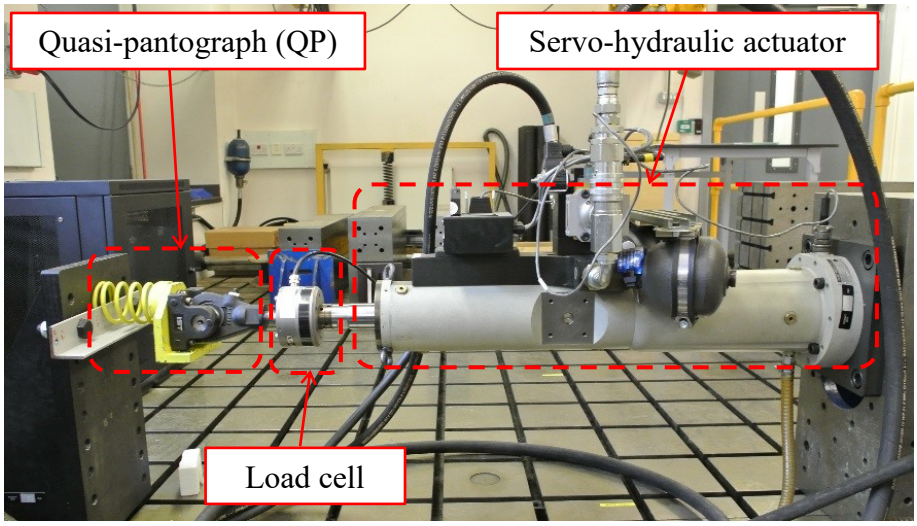

Figure 9. QP test rig in the ACTLab, University of Bristol.

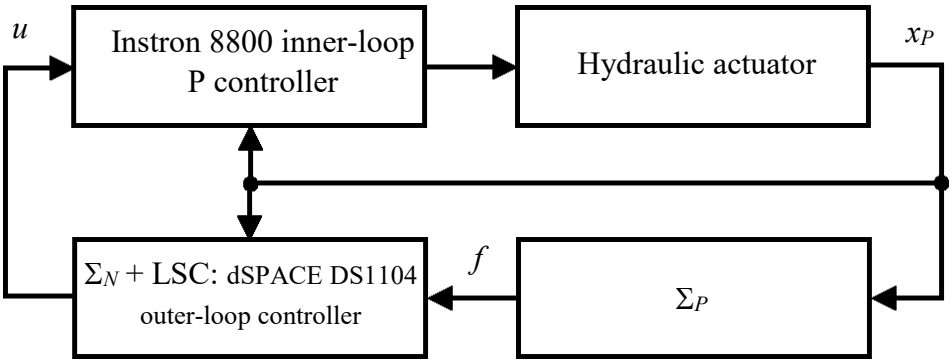

Figure 10. Block diagram of the QP-DSS-LSC test rig.

Parameter identification of the actuator and the QP

The dynamic parameters of the actuator, a and b, that appeared in equation (22) are required in the DSS design. These were estimated as $a \approx b \approx 54.0$, using the output error (**oe**) method within the System Identification Toolbox of MATLAB. Hence, the entries of the contact wire model parameter matrix, $\mathbf{A}_{N11}$ in equation (19), were determined as $A_{N11(i,i-1)} = A_{N11(i,i+1)} = 30.2$ and $A_{N11(i,i)} = -60.4$. Then, from equations (26) to (29) and equation (31), the LSC gains were computed as $K_{N1(i-1)} = K_{N1(i+1)} = 0.559$, $K_{N2(i)} = 0.0185$, $K_P = -0.118$ and $K_{e(i)} = 0.117$.

The measured displacement, x_p, and the estimated displacement based on the identified a and b are shown in Figure 11, where they are seen to have a good correspondence.

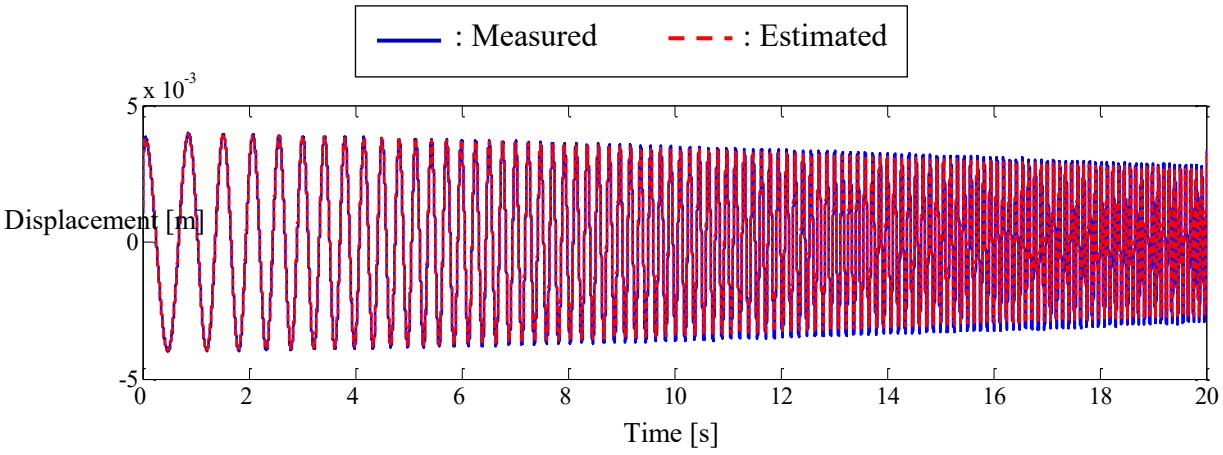

Figure 11. Comparison between measured and estimated output, x_P, based upon estimates of a, b.

The QP parameters m, c and k were identified in a similar manner, with $m \approx 6.18$ kg, $c \approx 29.1$ Ns/m and $k \approx 16700$ N/m. The experimentally measured displacement, x_p, and the estimated displacement based upon the identified parameters are shown in Figure 12, where they are again seen to have a good correspondence.

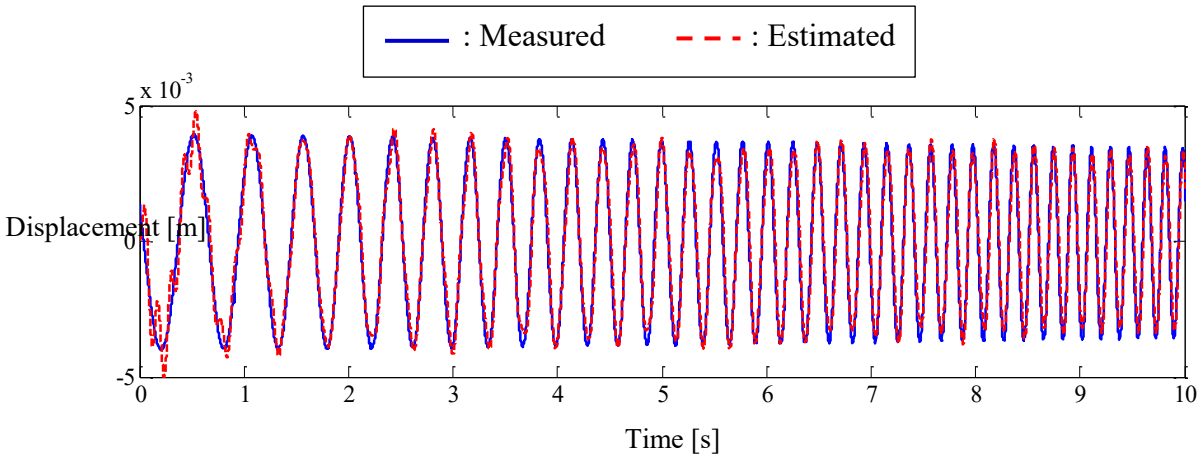

Figure 12. Comparison between measured and estimated output, x_P, based upon estimates of m, k, c.

Comparison of experimental and emulated system results

In this study, it is assumed that the QP runs under a catenary that is commonly used on high-speed railways in Japan and that the velocity of the QP is either 100 km/h, 200 km/h or 300 km/h. In this section, the modelled QP-catenary system (i.e. the benchmark *emulated* system) is simulated numerically for comparison with the DSS experimental system. The

emulated system response can be considered as a benchmark result for comparison purposes, since the emulated system uses complex contact and catenary wire models, neither of which are subject to the modal analysis or the moving window techniques. In DSS experimentation, the contact wire model was reduced in complexity by only using natural modes up to 14 Hz, so that the number of adopted eigenmodes in equation (3) was 30. The value of 14 Hz was an upper limit that proved to be a good compromise between complexity and accuracy of the model.

Figure 13 shows a comparison between the simulation results of the emulated system and the DSS experimentation, when the velocity of the QP was 100 km/h. It can be seen that they correspond well. Similarly, Figures 14 and 15 show the comparative results when the velocity of the QP was 200 km/h and 300 km/h, respectively. They, too, can be seen to correspond relatively well. However, it can also be seen that the simulated displacement and contact force of the emulated system has higher frequency components than those of experimental results. It is due to the reduction of dimension of the contact wire model, which is used for the DSS experimentation. Therefore, by adopting higher eigenmodes, the response of the DSS experiment could correspond closely with the emulated system. Our next phase of this work would be to reduce the computational load of the real-time simulation and to increase the number of adopted modes.

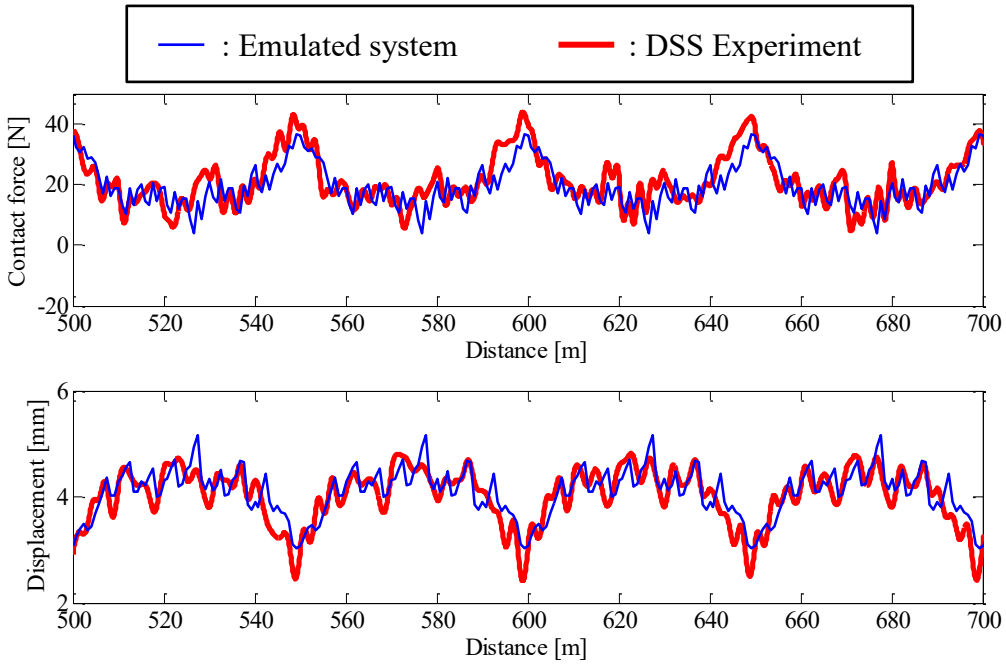

Figure 13. Comparison between experimental and emulated results (100 km/h).

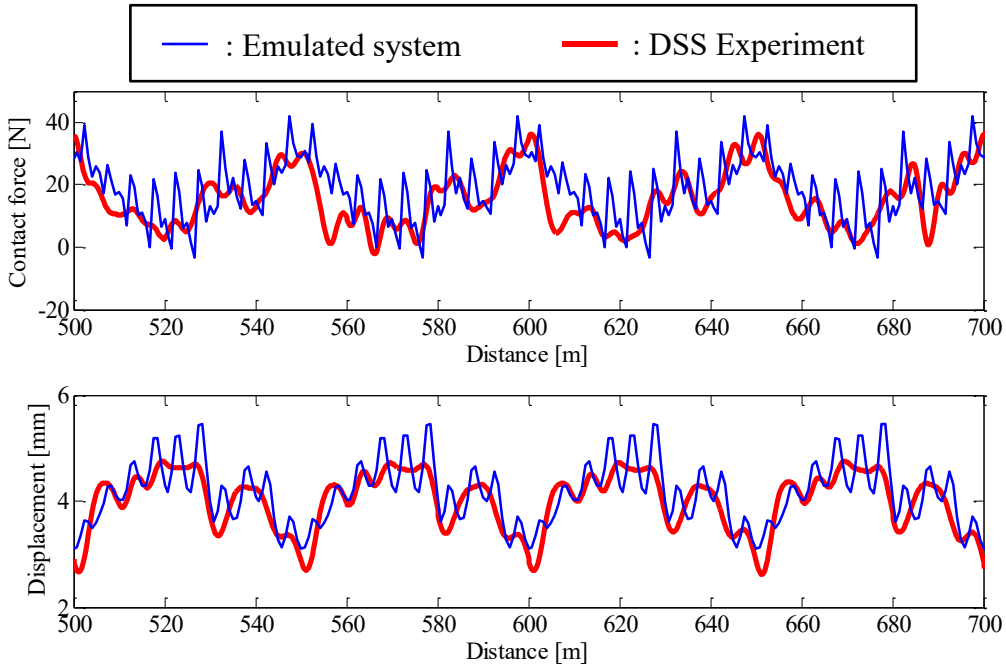

Figure 14. Comparison between experimental and emulated results (200 km/h).

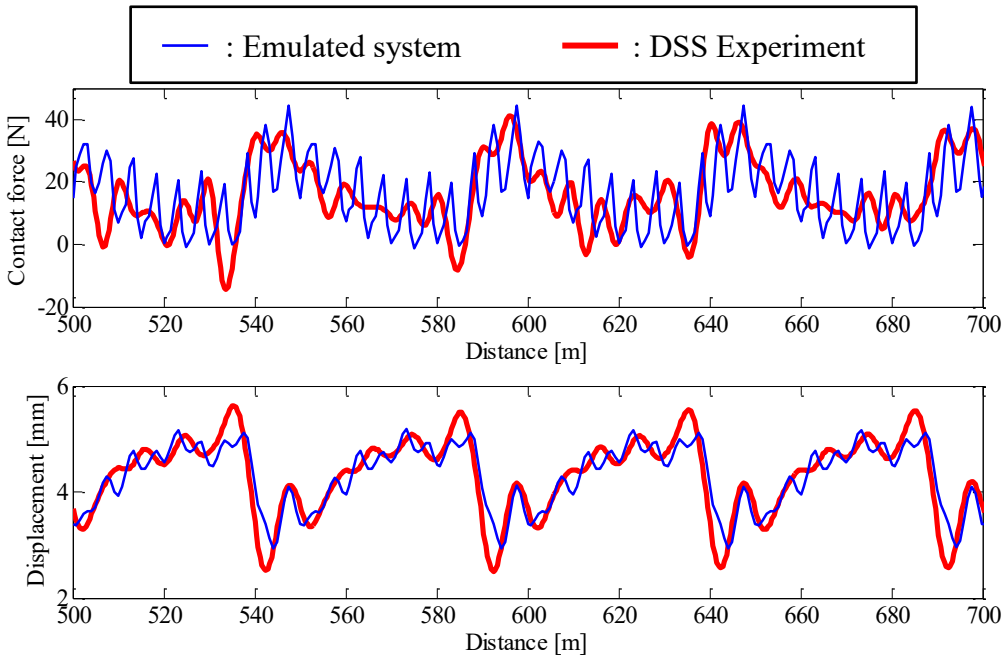

Figure 15. Comparison between experimental and emulated results (300 km/h).

Conclusions

A substructured test method for pantograph/catenary systems was developed, based upon the dynamically substructured system (DSS) approach of Stoten and Hyde[5]. In the DSS design, a linear substructuring control (LSC) method was used to synthesise the synchronising control law that rapidly reduced the displacement error between the physical pantograph head and the numerical catenary contact wire (at their point of contact) towards zero. In order to realise the real-time simulation of the catenary model, a modal analysis technique was adopted to reduce the dimension of the underlying model dynamics. Furthermore, a moving window approach was used to accommodate long-distance travel of the pantograph. This reduced a complex catenary model of length 1050 m (with 2500 states) to a series of 7 smaller catenary models, each of length 150 m (with 360 states). Moreover, each smaller catenary model was reduced to a 60-state model by the modal analysis technique, yielding an overall ~42-fold reduction in model complexity. The proposed method was validated by comparing responses of a benchmark emulated (i.e. overall) system simulation, with those of the DSS experiment.

Experiments were conducted within the Advanced Control and Test Laboratory (ACTLab), University of Bristol, using a simple mechanical quasi-pantograph (QP) system, under the condition that the QP runs at either 100 km/h, 200 km/h or 300 km/h. In the

100 km/h case, the experimental displacement and force at the point of contact between the QP head and the catenary contact wire corresponded very well with the simulated results. In the 200 km/h and 300 km/h cases, displacement and force outputs from the emulated system had higher frequency components than those of the experimental data, due to the modal reduction of the contact wire model. In future work, it is possible that the differences can be reduced by adopting a larger number of natural modes.

The next stage of this work is to validate the proposed DSS-LSC method on the pantograph testing rig at the Railway Technical Research Institute in Japan. Furthermore, the effect of the parameter variations within the servo-controlled actuator will be investigated. Finally, the effect of contact loss, catenary stagger and parameter variations within the catenary model, e.g. tension changes through the wires, are also to be investigated.

Declaration of Conflicting Interests

The author(s) declared no potential conflicts of interest with respect to the research, authorship, and/or publication of this article.

Funding

The author(s) received no financial support for the research, authorship, and/or publication of this article.

References

[1] Kurita T. Development of external-noise reduction technologies for shinkansen high-speed trains. *Proc JSME: Journal of Environment and Engineering 2011*; 6: 805-819.

[2] Kobayashi S, Yamashita Y, Ikeda M, Masuda A and Iba D. Control parameter optimization of active control pantograph based on steepest descent method. In *Proceedings of the 10th World Congress Railway Research (WCRR2013), Sydney, Australia*, 25-28 November 2013.

[3] Koyama T, Usuda T, Kawasaki K, Nakamura K and Kawamura T. Methods for detecting pantograph defects using sensors installed on contact lines. *Quarterly Report of RTRI* 2016; 57: 207–212.

[4] Song Y, Liu Z, Wang H, Lu X and Zhang J. Nonlinear modelling of high-speed catenary based on analytical expressions of cable and truss elements. *Vehicle System Dynamics* 2015; 53: 1455–1479.

[5] Song Y, Liu Z, Wang H, Lu X and Zhang J. Nonlinear analysis of wind-induced vibration of high-speed railway catenary and its influence on pantograph–catenary interaction. *Vehicle System Dynamics* 2016; 54: 723–747.

[6] Song Y, Liu Z, Duan F, Lu X and Wang H. Study on Wind-Induced Vibration Behavior of Railway Catenary in Spatial Stochastic Wind Field Based on Nonlinear Finite Element Procedure. *Journal of Vibration and Acoustics* 2018 140: 011010.

[7] Nåvik P, Rønnquist A and Stichel S. The use of dynamic response to evaluate and improve the optimization of existing soft railway catenary systems for higher speeds. *Proc. IMechE Part F: J. Rail and Rapid Transit 2015*; 230: 1388-1396.

[8] Nåvik P, Rønnquist A and Stichel S. Variation in predicting pantograph–catenary interaction contact forces, numerical simulations and field measurements. *Vehicle System Dynamics* 2017; 55: 1265–1282.

[9] Van OV, Massat JP and Balmes E. Waves, modes and properties with a major impact on dynamic pantograph-catenary interaction. *Journal of Sound and Vibration* 2017; 402: 51-69.

[10] Song Y, Liu Z, Duan F, Xu Z and Lu X. Wave Propagation Analysis in High-speed Railway Catenary System Subjected to a Moving Pantograph. Applied Mathematical Modelling 2018; 59: 20-38.

[11] Ikeda M. 'Gasen-do FE' statement of methods. *Vehicle System Dynamics* 2015; 53: 357–369.

[12] Stoten DP and Hyde RA. Adaptive control of dynamically substructured systems: the ingle-input single-output case. *Proc. IMechE Part I: J. Systems and Control Engineering 2006*; 220: 63-79.

[13] Stoten DP. A comparison of hybrid and DSS schemes for substructured system testing. In *Proceedings of the 12th International Conference on Motion and Vibration Control (MOVIC 2014), Hokkaido, Japan*, 3-7 August 2014.

[14] Facchinetti A, Gasparetto L and Bruni S. Real-time catenary models for the hardware-in-the-loop simulation of the pantograph–catenary interaction. *Vehicle System Dynamics* 2013; 51: 499–516.

[15] Schirrer A, Aschauer G, Talic E, Kozek M and Jakubek S. Catenary emulation for hardware-in-the-loop pantograph testing with a model predictive energy-conserving control algorithm. Mechatronics 2017; 41: 17-28.

[16] Yamashita Y, Usuda T and Kobayashi S. Application of dynamically substructured systems scheme to parametric excitation system intended to HILS test procedure for catenary pantograph system. In *Proceedings of the 22nd United Symposium for Railway Technology, Tokyo, Japan*, 9-11 December 2015.

[17] Stoten DP, Yamaguchi T and Yamashita Y. Dynamically substructured system testing for railway vehicle pantographs. In *Proceedings of the 12th International Conference on Motion and Vibration Control (MOVIC 2014), Southampton, United Kingdom*, 3-6 July 2016.

[18] Kobayashi S, Stoten DP, Yamashita Y and Usuda T. Substructured testing for pantograph/overhead catenary systems based on dynamically substructured systems. In

Proceedings of the Railway Engineering 2017, Edinburgh, United Kingdom, 21-22 June 2017.

[19] Tu J, Stoten DP, Hyde RA and Li G. A state-space approach for the control of multivariable dynamically substructured systems, *Proc. IMechE Part I: J. Systems and Control Engineering 2011*; 225: 935-953.